Proceedings of ASME Turbo Expo 2011
GT2011
June 6-10, 2011, Vancouver, British Columbia, Canada

GT2011-45314

COMPUTATION OF INGESTION THROUGH GAS TURBINE RIM SEALS

Kunyuan Zhou* **Mike Wilson** **J Michael Owen**
Gary Lock

* Dept of Engineering Thermophysics
School of Jet Propulsion
Beihang University
Beijing, 100191 P.R.China

Dept of Mechanical Engineering
University of Bath
Bath, BA2 7AY
United Kingdom

ABSTRACT

Three-dimensional unsteady computational fluid dynamics (CFD) is applied to the ingestion of fluid from a non-uniform mainstream annulus flow via a rim-seal into a rotor-stator wheel-space. The results provide understanding of the complex flow and information for the development of more efficient computational models and analytical 'orifice models'.

The commercial CFD code CFX has been used to carry out unsteady RANS computations with an SST turbulence model. A scalar equation is employed to represent the seeded tracer gas that can be used in experiments to determine sealing effectiveness, and the variation of effectiveness with sealing flow rate is determined for a simple axial clearance seal and one combination of axial and rotational Reynolds numbers. The computational domain comprises one pitch in a row of stator vanes and rotor blades The rotating blade is accounted for by a sliding interface between the stationary and rotating sections of the model, located downstream of the seal clearance.

The unsteady computations confirm that the magnitude of the peak-to-trough pressure difference in the annulus is the principal driving mechanism for ingestion (or ingress) into the wheel-space. This pressure difference is used in orifice models to predict sealing effectiveness; its magnitude however depends on the locations in the annulus and the wheel-space that are chosen for its evaluation as well as the sealing flow rate. The CFD is used to investigate the appropriateness of the locations that are often used to determine the pressure difference. It is shown that maximum ingestion occurs when the static pressure peak produced by the vane combines with that produced by the blade, and that highly swirled ingested flow could contact both the stator and rotor disk when little sealing flow is provided.

The relationships between the unsteady simulations and simplified, more computationally efficient steady computations are also investigated. For the system considered here, ingress is found to be dictated principally by the pressure distribution caused by the vane. The effect of the rotating blade on the pressure distribution in the annulus is investigated by comparing the unsteady results with those for steady models that do not involve a blade. It is found that the presence of the blade increases the pressure asymmetry in the annulus. Although the pressure asymmetry predicted by unsteady and steady models have a similar magnitude, the sealing effectiveness is over-predicted considerably for the corresponding steady model. If a "thin seal" geometric approximation is used in the steady model, however, similar effectiveness results compared with the unsteady model may be obtained much more economically.

NOMENCLATURE

b	radius of seal
c	concentration
C_p	pressure coefficient [$= (p_2 - \bar{p_2}) / (^1/_2\, \rho\Omega^2 b^2)$
C_w	nondimensional flow rate ($=\dot{m}/\mu b$)
$C_{w,min}$	minimum value of $C_{w,o}$ to prevent ingress
$C_{w,o}$	nondimensional sealing flow rate
G_c	seal-clearance ratio ($=s_c/b$)
$\dot{m}$	mass flow rate
p	static pressure
$\bar{p}$	mean absolute static pressure over one vane pitch
r	radius
Re_W	axial Reynolds number in annulus ($=\rho Wb/\mu$)
Re_ϕ	rotational Reynolds number ($=\rho\Omega b^2/\mu$)
s	axial gap between rotor and stator in wheel-space
s_c	axial seal clearance
t	time
t_{bpp}	time for one blade passing period
u_t	friction velocity ($=(\tau_w/\rho)^{1/2}$)
U	bulk mean radial velocity component of sealing air through the seal clearance

V_r, V_ϕ	radial and tangential components of velocity
W	axial velocity in annulus
y	distance of near-wall node from wall surface
$y+$	nondimensional wall distance ($=yu_t\rho/\mu$)
z	axial distance to the stator wall
β	swirl ratio ($=V_\phi/\Omega r$)
Δp	peak-to-trough pressure difference in annulus ($=p_{2,max} - p_{2,min}$)
ε	computed effectiveness ($=(c_s-c_a)/(c_o-c_a)$)
Φ_o	nondimensional sealing parameter($=C_{w,o}/2\pi G_c Re_\phi$)
Φ_{min}	value of Φ_o when $C_{w,o}=C_{w,min}$
Γ_c	empirical parameter in orifice model equation
μ	dynamic viscosity
θ	normalized tangential coordinate between vanes
ρ	density
σ_{Cp}	standard deviation in unsteady C_p distribution
τ_w	wall shear stress
Ω	angular speed of rotating disc

Subscripts

a	value in annulus
EI	externally-induced (ingress)
max	maximum
min	minimum
o	superposed (sealing) flow;
s	value on stator
$1,2$	locations in wheel-space and annulus

1. INTRODUCTION

The minimum sealing air flow needed to prevent overheating of the rotor-stator wheel-spaces in gas turbines is a major concern today. Too much sealing air would reduce the overall engine efficiency, which is harmful for carbon dioxide emissions to the environment; too little air could lead to over-heating and catastrophic failure. Therefore, it is important to understand the mechanisms of annulus hot gas ingestion (ingress) into the rotor-stator wheel-space to assist engine designers in determining the best seal geometry for the minimum use of sealing air.

This present work aims to improve understanding of the fundamental physics of ingress using 3D unsteady computational fluid dynamics (CFD). Results have also been obtained using two different 3D steady computational models. The study was carried out prior to an experimental investigation, to be reported elsewhere [1, 2] and the computed flow field information has been used to inform and interpret the experiments.

Owen et al. [3] developed an 'orifice model', which was used to predict the effectiveness, ε, of rim seals. The model provided implicit analytical solutions for both rotationally-induced (RI) ingress, where the rotating flow in the wheel-space created the dominant driving force for ingestion, and externally-induced (EI) ingress, where the circumferential pressure distribution in the annulus was the principal driving force. For EI ingress, it was assumed that ingress occurred where the pressure in the annulus was higher than that in the wheel-space and egress occurred where it was lower.

In [3], the sealing flow parameter was defined as:

$$\Phi_o = \frac{C_{w,o}}{2\pi G_c Re_\phi} \tag{1}$$

As both Re_ϕ and $C_{w,o}$ include the viscosity, which cancel in eq (1), an alternative (though equivalent) definition for Φ_0 is:

$$\Phi_o = \frac{U}{\Omega b} \tag{2}$$

where U is the bulk mean of the radial component of velocity of sealing air through the seal clearance, i.e.:

$$U = \frac{\dot{m}_o}{2\pi\rho b s_c} \tag{3}$$

Eq (2) shows that Φ_0 is an inertial parameter.

Sangan et al. [2] give explicit solutions of the orifice model, for both rotationally-induced and externally-induced ingress, for the variation of ε with Φ_0 . For EI ingress, which is the subject of this paper, the 'effectiveness equation' is

$$\frac{\Phi_o}{\Phi_{min,EI}} = \frac{\varepsilon}{[1+\Gamma_c^{-2/3}(1-\varepsilon)^{2/3}]^{3/2}} \tag{4}$$

where Φ_{min} is the minimum value of Φ_0 for which the system is sealed, i.e. so that $\varepsilon=1$ when $C_{w,0} = C_{w,min}$. Γ_c is the ratio of the discharge coefficients for ingress and egress in the orifice model and is an empirical parameter. Figure 1 shows a typical theoretical variation of ε with Φ_0 according to eq (4), for a case where $\Phi_{min,EI}$ = 0.348 and Γ_c = 0.37 (Zhou et al. [4] show the effect of varying Γ_c as a parameter). As Φ_0 increases, the sealing effectiveness increases until $\varepsilon = 1$ after which no ingestion occurs.

The preliminary results of steady computations were also presented in [3]. These computations utilised a "thin seal" geometric approximation to create realistic levels of ingestion, and the computed variation of ε with Φ_0 was shown to be consistent with the predictions from the orifice model. The unsteady computations described in the present paper are an extension of this work.

Owen et al. also gave an overview of findings from previous computational studies, including those by Hills et al. [5], Laskowski et al. [6], Rabs et al. [7], Johnson et al. [8], Wang et al. [9], Zhou et al. [10], Lewis and Wilson [11] and Mirzamoghadam et al. [12, 13]. Decisions on some of the modelling approaches employed in the present work were made taking these findings into consideration.

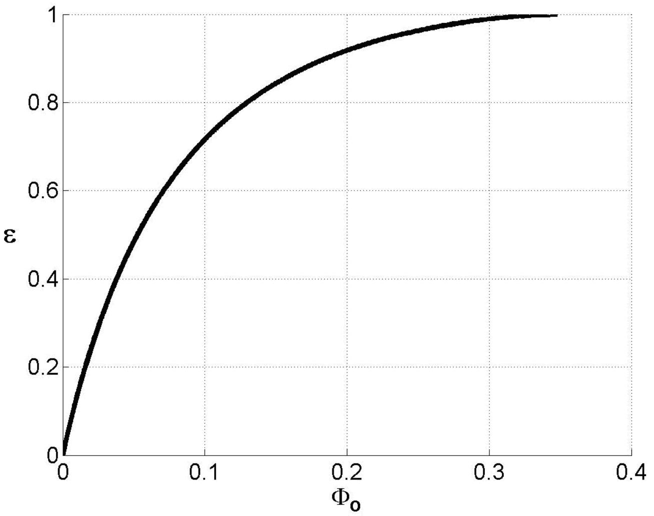

Figure 1 Typical theoretical variation of sealing effectiveness ε with sealing flow parameter Φ_0 according to eq (4)

More recent unsteady computations of ingestion have been reported by O'Mahoney et al. [14] , Julien et al. [15] and Dunn et al. [16]. Dunn et al. investigated the sensitivity of a 1/14th sector model (incorporating four stator vanes and four rotor blades and involving an overlapping radial seal) to two different mesh distributions (having 1.1 and 2.1 million mesh cells) and two different turbulence models (Spalart-Allmaras and realizable k-ε). The results were used to argue that large scale structures would contribute to ingestion, though it was concluded that these were constrained by the 1/14th sector used for the computations and that further time iterations were also required. Julien et al. [15] carried out unsteady ingress computations for a 72 degree sector model, and found that energetic large scale unsteady flow structures existed in the wheel-space at smaller purge (sealing) flow rates that augmented ingestion through pressure perturbations. These effects were found to be inhibited by increasing the purge flow rate. O'Mahoney et al. [14] used unsteady Reynolds-averaged Navier-Stokes (URANS) computations and Large Eddy Simulation (LES) to study rim seal ingestion for a chute seal geometry. They compared computational results to previously published experimental data and found that the LES results gave better agreement for the prediction of the sealing effectiveness than the URANS approach. However, the LES approach required very large computational resources (512 CPUs for 14 days) for a section model only. As noted by Dunn et al [16], this is too expensive currently for engineering applications.

The effect of blades on ingestion was studied experimentally by several research teams. Green et al. [17] showed the blades to have a positive effect in *reducing* ingestion. By contrast, Bohn et al. [18] found the opposite effect, which was attributed to the increase of average static pressure asymmetry in the annulus due to the presence of the blades.

In the present paper, unsteady RANS computations are carried out using the modified SST turbulence model by Menter et al. [19]. Three different computational models have been studied, two of which are steady models without a blade. One of the steady models uses the seal with the actual radial depth while the other uses the 'thin seal' approximation as described by Owen et al. [3] and which is explained fully below.

Computational models and convergence information are given in section 2. Computed results for the annulus and the wheel-space are presented and discussed in sections 3 and 4 respectively. Sealing effectiveness results are discussed in section 5. Concluding remarks and prospects for future work are given in section 6.

2. COMPUTATIONAL MODEL

The commercial software package CFX V11.0 is employed for this study. The geometry (not to scale) and boundary conditions are illustrated in Figure 2(a). The model (including the vane and blade geometries) is based on the design of an experimental rig at the University of Bath described by Sangan et al. [1]. The rig contains 32 stator vanes and 41 rotor blades, however for simplicity a configuration of 32 vanes and 32 blades has been studied computationally. Hence, an 11.25 degree sector model is considered, having one vane and one blade in the mainstream annulus. The annulus height is 10mm. The axial spacing between the vane trailing edge and the blade leading edge is 12mm. An axial clearance seal is located midway between the vane trailing edge and the leading edge of the blade. The wheel-space gap between rotor and stator is s = 20mm and the seal axial clearance is s_c = 2mm. The wheel-space outer radius is b = 190mm. A compact wheel-space is modeled, truncated using a stationary inner shroud. This reduces computation times and helps focus the study on the flow field in the vicinity of the seal.

ICEM CFX 11.0 was employed to generate hexahedral meshes for both steady and unsteady models. Figure 2(b) illustrates mesh details for the steady model; this model does not involve a rotating blade and is the model described by Owen et al. [3]. Figure 2(c) shows the relevant modifications for the unsteady model. The rotating blade is a symmetric NACA 0018 aerofoil, as used in the experimental rig (Sangan et al. [1]) to avoid the need for an absorption dynamometer. The unsteady model contains 2.2 million nodes and 2.1 hexahedral elements. Mesh independence checks were carried out (in the range 1.37 million to 2.33 million nodes in total) for the annulus pressure distribution downstream of the vane trailing edge and for the radial distribution of effectiveness in the wheel-space. The $y+$ values were less than 2 in the wheel-space where the reference point for calculating the effectiveness was taken, and $y+_{max} \approx$ 20 and 40 was observed in the vane and blade region respectively. The expansion ratio between successive grid nodes was not greater than 1.2.

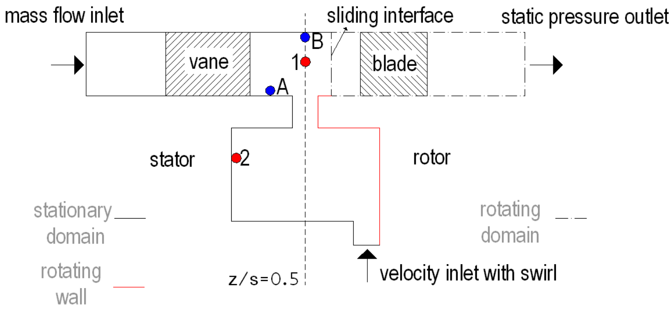

(a) Geometrical model (not to scale) and boundary conditions

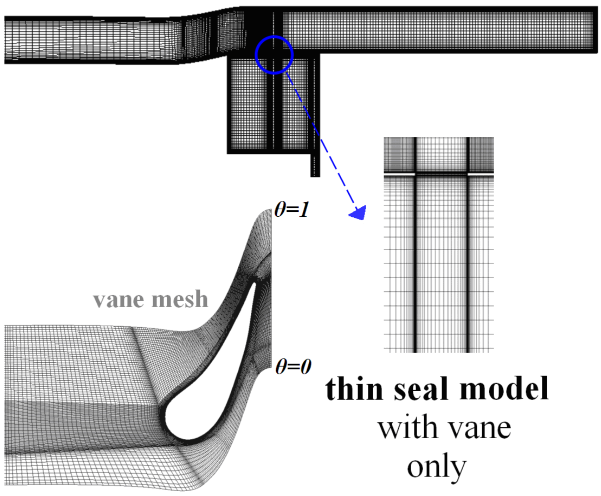

(b) steady computations

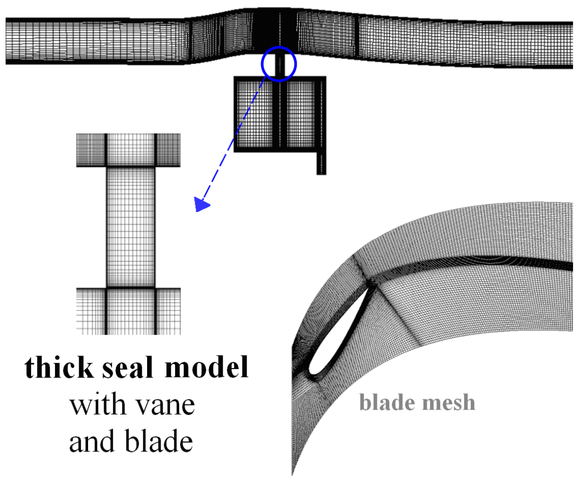

(c) unsteady computations

Figure 2. Computational model and mesh details

The unsteady RANS equations with the SST turbulence model were solved in the computations. Upwinding was used for the advection terms and the second order backward Euler scheme was used for the transient calculations. The residual target for unsteady simulations was that the normalized RMS error for each conservation balance over the entire mesh fell to less than 10^{-4}.

The time step used was 2.3×10^{-5}s, corresponding to 20 time steps for each blade passing period (*bpp*). The instant when the rotor blade leading edge is aligned with the vane trailing edge (in the axial direction) is taken as the starting point for the transient data presentation, i.e $t/t_{bpp} = 0$. Converged "frozen rotor" results were taken as the initial values for the unsteady calculations. 32 computational cells were used to resolve the vane passage in the tangential direction.

A sliding interface is located 2mm downstream of the axial clearance seal trailing edge for the exchange of information between the stationary and the rotating frame. (The location chosen for the interface was guided by recommendations made by Mirzamoghadam et al. [10]). Mass flow rates are prescribed at both the annulus inlet and the superposed sealing flow inlet. The average gauge static pressure is set to be zero at the outlet (an absolute static pressure of 1 bar and ambient static temperature of 298 K was used to calculate reference values for fluid properties). The mass concentration of the tracer is 1 at the sealing flow inlet and 0 and the annulus flow inlet. Cyclic symmetry conditions are applied at the circumferential faces of the sector model.

The parameters used for the computations are shown in Table 1. As shown in Figure 1, the values of Φ_0 chosen for the unsteady computations correspond to sealing flow rates expected to give rise to low, medium and high values of sealing effectiveness.

Re_ϕ	Re_w	G_c	$\dot{m}_o/\dot{m}_a$	$C_{w,o}$	Φ_0
10^6	8×10^5	0.01	0.5%	1.44×10^3	0.022
			2.5%	7.19×10^3	0.11
			5%	1.44×10^4	0.22

Table 1 Conditions for the unsteady computations

A detailed description of a steady computational model (having the same stator vane and wheel-space geometry as that used here but with no blade, as shown in Figure 2(b)) was given by Owen et al. [3]. This model employed a "thin seal" geometric approximation as described above. Results from that steady model are discussed in this paper, as well as steady flow results obtained for a model having the true seal geometry (as used in the unsteady model). The difference between the "thin seal geometry" and the true seal geometry can be seen in Figure 2 (b) and Figure 2(c). For convenience in this paper, the steady model with the true seal geometry is referred to as the "thick seal steady model"; the steady model with the thin seal approximation is termed the “thin seal steady model”. The steady computations all converged to normalized residual levels below 10^{-6}.

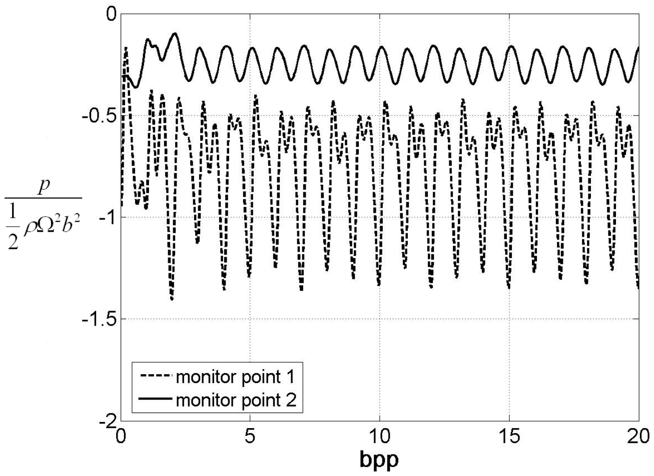

(a) Static pressure convergence history

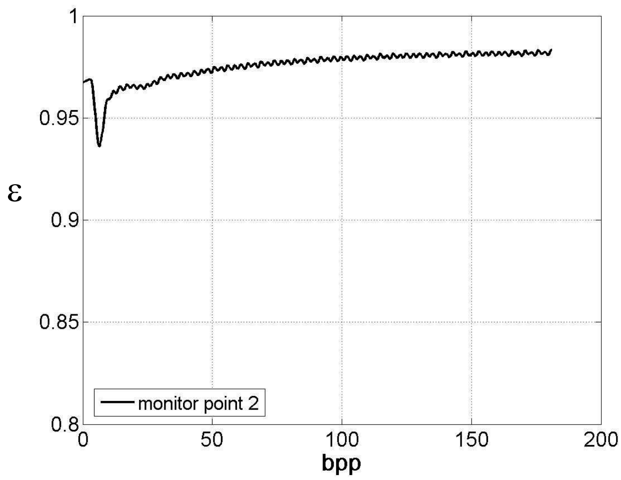

(b) Effectiveness convergence history

Figure 3. convergence history for thick seal unsteady model for Φ_0 = 0.22
(monitor points 1 and 2 are shown in Figure 2(a))

As shown in Figure 3(a), for the unsteady model when Φ_0 = 0.22, the chosen monitor values of static pressures in the annulus and in the wheel-space (at the locations 1 and 2 respectively shown Figure 2(a)) become quasi-periodic in less than 20 blade passing periods. This indicates that the flow field converges in less than one rotor revolution. However, for convergence of the sealing effectiveness at the monitor point 2 on the stator wall, more than 100 blade passing periods (3 full rotor revolutions) are required, the time for convergence depending on the initial conditions and the sealing flow rate. The effectiveness was taken to be converged when the change at the monitor point becomes relatively small (less than 0.2% relative difference between the ensemble average value of the last 10 bpps and that of the previous 10 bpps). An example of the convergence history is shown in Figure 3(b). Each unsteady computation required more than 216 hours to converge using 8 × 2.8GHz CPUs in parallel, compared with 10 hours for each steady case (using the same resources).

3. COMPUTATIONS IN THE ANNULUS

The locations at which static pressure can be measured in experiments are normally limited. Two such representative locations are chosen here to present the time averaged results of computations. One is on the stator hub half way between the vane trailing edge and the stator-side edge of the seal (Location A). The other is on the annulus wall radially outward of the axial centre of the seal clearance (Location B). Locations A and B are illustrated in Figure 2(a).

Figure 4 (a) and (b) show the computed circumferential distribution of time average static pressure in one vane pitch for the unsteady model over one blade passing period, at locations A and B respectively for the three different values of Φ_0. (The values of ε shown in Fig 4 correspond to the results of the unsteady computations and are discussed in section 5.) The figures show that the effect of increasing sealing flow is to reduce the maximum value and the magnitude of the variation of the annulus pressure distribution. This is consistent with findings reported by Bohn et al. [20]. The peak-to-trough pressure at location B is approximately two thirds of that at location A; however, the circumferential locations of the maximum and minimum pressure values at the two locations are nearly the same. Similar trends are observed for the steady results. These results suggest that, except for the smaller magnitude of the asymmetry at location B, circumferential pressure distributions measured either on the stator platform or on the annulus wall above the seal clearance in an experiment will give a similar indication of the signature pressure variations contributing to ingestion.

Figure 5 shows the comparison between circumferential distributions of non-dimensional static pressure at location A for all three models at Φ_0 = 0.22. This high sealing flow rate case was chosen as this identifies most clearly the causes of ingestion. The result for the unsteady model is the time average value over one blade passing period; the magnitude of the standard deviation σ_{Cp} about this time average is also illustrated. The magnitude of σ_{Cp} indicates the size of the pressure fluctuations in the unsteady computations. These fluctuations create ingestion that is additional to that created by the time-average distribution of pressure.

Similar time-average static pressure distributions are predicted by all the models. The unsteady computation gives rise to a greater average peak-to-trough variation compared with the steady results, due to the unsteady pressure produced by the blade. The thin seal approximation has little impact on the computed steady flow pressure distribution. The pressure peak location in all three results is close to the vane trailing edge location although biased toward the pressure surface. The general agreement between the time-averaged unsteady and steady results shows that the time-averaged static pressure distribution at this location is due mainly to the flow field caused by the vane.

Figure 6(a) shows contours of static pressure for the thin seal steady model at 5% radial height of the annulus above the stator hub. (There was little difference in the static pressures and radial velocities near the seal gap between the two steady models.) The radial velocity distribution at the outer radius of the seal clearance is also shown.

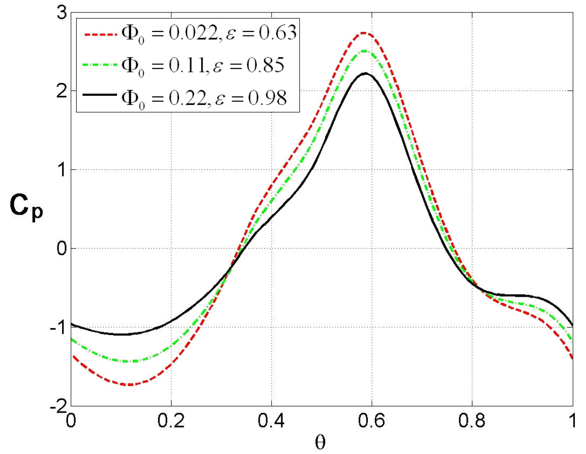

(a) location A: stator hub

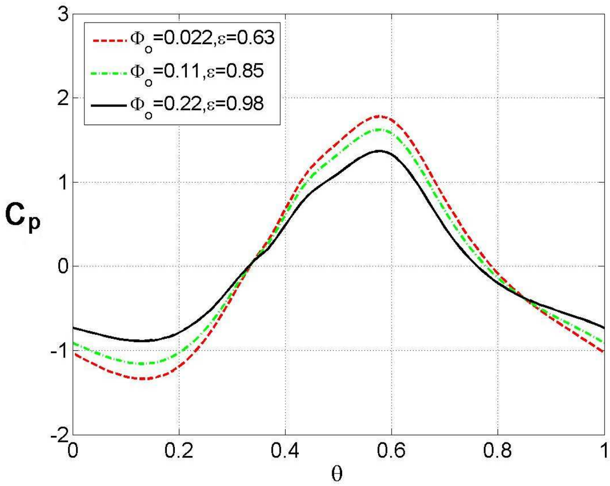

(b) location B: annulus wall radially outward of the seal clearance axial centre (z/s = 0.5)

Figure 4. Computed time average circumferential distributions of static pressure for the unsteady computations

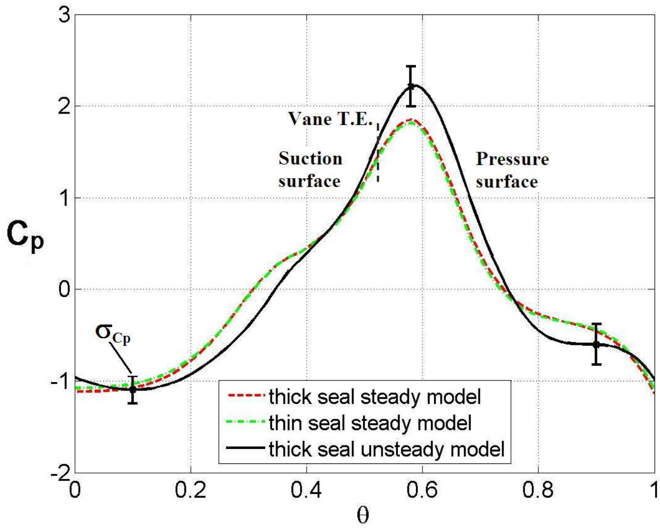

Figure 5. Computed circumferential distribution of static pressure at location A for three different models, $\Phi_0 = 0.22$

Red contours in the seal clearance region indicates ingress ($V_r < 0$), while blue represents areas with egress ($V_r > 0$). For the pressure contours, red represents higher pressure and blue represents lower pressure. The figure shows that ingestion occurs first where the static pressure is relatively high, and persists in the direction of the swirl. The flow from the wheel-space tends to impinge on the annulus flow at relatively low pressure regions. The ingested fluid is drawn from the region immediately upstream of the seal clearance, and ingestion is driven initially by the relatively high pressure in this region. These observations are consistent with the assumptions made in the orifice model [3] that the principal driver for EI ingress is the circumferential distribution of pressure in the annulus.

Figure 6(b) and (c) show corresponding results at two different instants (hence two different locations of the blade relative to the vane) for the unsteady computation. The direction of rotation of the disc is indicated in the figures. Again the system is nearly sealed at $\Phi_0 = 0.22$. As the annulus pressures change with time, two extreme instants are shown. Figure 6(b), for the instant at $t/t_{bpp} = 0.05$, shows that maximum ingestion occurs when the pressure peak due to the vane interacts with that produced by the rotating blade. Figure 6(c), for $t/t_{bpp} = 0.55$, shows that when the vane pressure peak is counteracted by the blade pressure trough only two very small regions of inward flow in the seal clearance region can be identified. This accords with the two high pressure regions produced by the vane and the blade.

Both the steady and the unsteady computations show that inflow and outflow at the seal clearance follows the circumferential pressure variation in the annulus. However, it is shown below that the flow entering the seal clearance from the annulus is not necessarily ingested into the wheel-space.

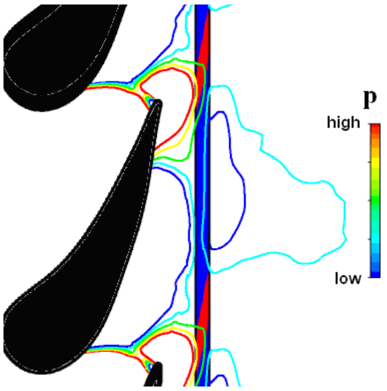

(a) thin seal steady model

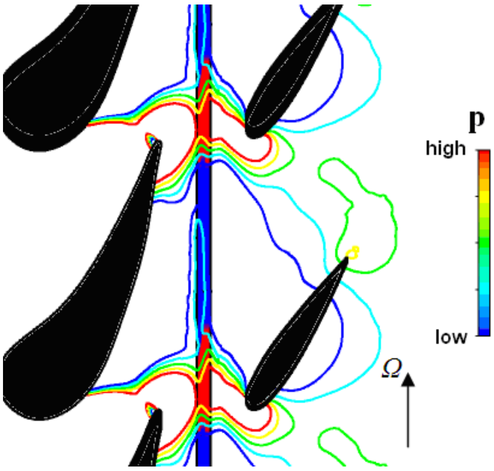

(b) unsteady model, t/t_{bpp}= 0.05

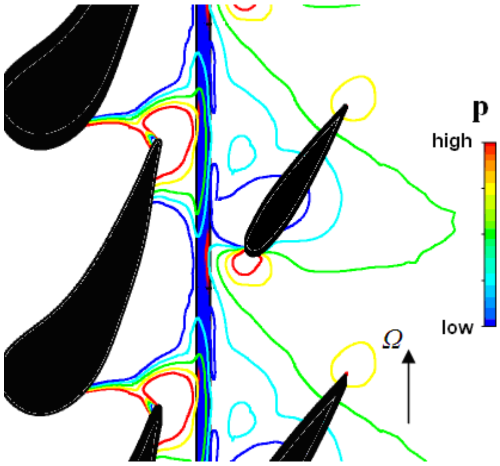

(c) unsteady model, t/t_{bpp}= 0.55

Figure 6. Line contours of static pressure in the z-θ plane at 5% annulus height and radial velocity contours in the seal clearance (red - inward radial velocity, blue - outward radial velocity) for Φ_0 = 0.22 (t/t_{bpp}= 0 is defined as the instant when the blade leading edge is aligned with vane trailing edge in the axial direction)

4. COMPUTATIONS IN THE WHEEL-SPACE

Figure 7 shows computed streamlines and contours of effectiveness for the thick seal steady model in the r-θ plane at the middle axial plane of the seal clearance (z/s = 0.5 for the rotor-stator wheel-space) for Φ_0 = 0.022, (The direction of rotation of the disc is indicated on the figures.) This low sealing flow rate case was chosen as the computed effectiveness results can be more clearly distinguished for the three different models. The streamlines show that flow from the annulus enters the seal region for $0.5 < \theta < 1$ approx. but that, rather than entering the wheel-space, flow is subsequently radially outward in the direction of rotation ($0 < \theta < 0.5$). A recirculation within the seal in this steady model computation prevents the annulus flow entering the wheel-space (see Lewis and Wilson [11] and Bohn et al. [21]). As a consequence, even at this low sealing flow rate, the contours of computed effectiveness in the wheel-space show values to be close to unity, indicating that very little ingestion occurs.

Figure 8 shows the streamline and effectiveness contours at the same sealing flow rate Φ_0 = 0.022 for the thin seal steady model. Annulus flow is again drawn in to the seal region as for the thick seal model. However, since the radial thickness of the seal is reduced almost to zero in the thin seal approximation, the fluid enters the wheel-space as it flows in the direction of rotation. The thin seal approximation allows ingestion to occur by inhibiting the formation of the recirculation within the seal. Values of effectiveness over much of the wheel-space (at this circumferential location) are around 0.3, due to strong mixing between the ingested flow and the sealing flow. This mixing is augmented by the rotor-stator recirculation in the wheel-space.

Figure 9 (a), (b), (d) and (e) show further computed streamlines and contours of effectiveness at two circumferential planes (θ = 0 and θ = 0.5) for the thin seal steady model for this low sealing flow rate case. It can be seen that, at both locations, fluid ingested from the annulus mixes with the flow on both the rotor and stator sides of the wheel-space. Since the swirl ratio (β) of the ingested flow is greater than 1, the ingested fluid would be expected to travel radially inward on both the rotor and stator surfaces, see Owen and Rogers [22]. The dashed line in the figures shows the approximation location where β = 1. The lower values of effectiveness toward the rotor side suggest that ingested fluid is drawn mainly into the rotor-side recirculation shown in the streamlines. Figure 9(c) and (f) shows time average contours of effectiveness in the r-z plane for the thick seal unsteady model at θ = 0 and θ = 0.5 respectively. It can be seen that the unsteady thick seal model gives higher predicted effectiveness (less ingestion) than the thin seal steady model.

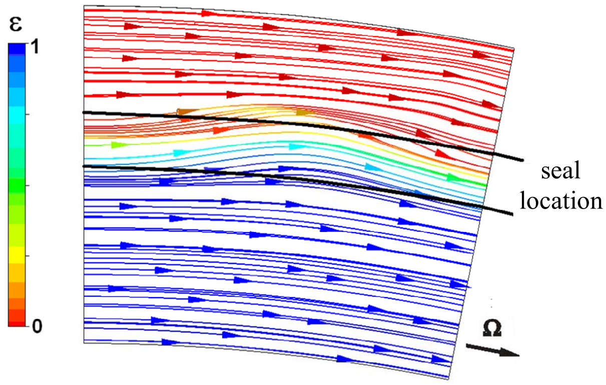

(a) streamlines

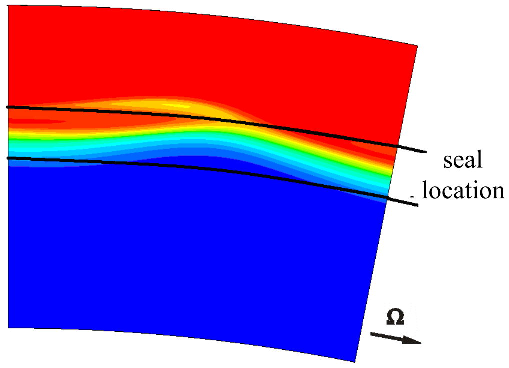

(b) contours of effectiveness

Figure 7. Computed results in the r-θ plane at z/s = 0.5 (axial centre plane of the seal clearance) for Φ_0 = 0.022, thick seal steady model

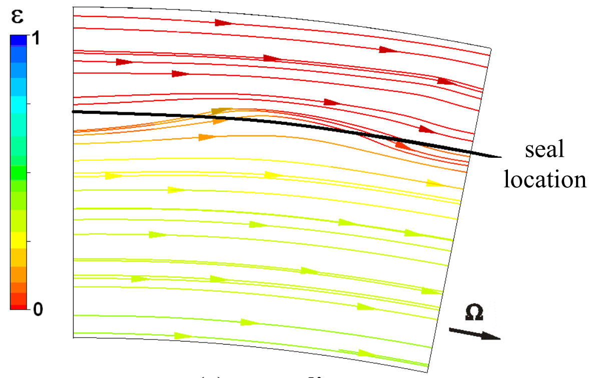

(a) streamlines

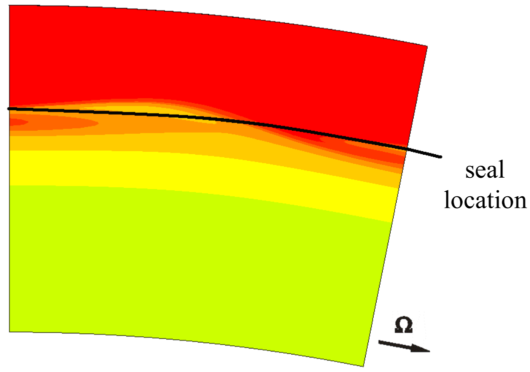

(b) contours of effectiveness

Figure 8. Computed results in the r-θ plane at z/s = 0.5 (axial centre plane of the seal clearance) for Φ_0 = 0.022, thin seal steady model

Figure 10 shows instantaneous computed contours of effectiveness in the r-θ plane at z/s = 0.5 for the unsteady computation, once again for Φ_0 = 0.022. Compared with the thick seal steady model result shown in Fig. 7(b), there is a more coherent and more localized recirculation within the seal that brings annulus flow into the wheel-space progressively over one blade passing period. In addition to this advection into the wheel-space, there is turbulent mixing between the annulus flow and the sealing flow in the vicinity of the seal.

Figure 11 (a-c) shows computed time average effectiveness contours at the low, medium and high values of Φ_0 respectively for the unsteady computations. As Φ_0 increases, the overall effectiveness in the wheel space is increased. There is qualitative agreement between Fig 11(a) and Figure 7(b) for the *location* of regions of most ingestion into the seal region for Φ_0 = 0.022, although the *amount* of ingestion into the wheel-space is different. Much more ingestion into the wheel-space occurs for the thin seal steady model for this case (Figure 8(b)).

5 SEALING EFFECTIVENESS

The computed variation of effectiveness in the wheel-space (at the monitor location 2 shown in Figure 2a) with Φ_0 is shown in Figure 12. The more well-defined recirculation in the seal clearance predicted by the unsteady computations encourages ingestion and its further penetration into the wheel-space. This gives rise to lower levels of effectiveness than for the thick seal steady model, which produces very little ingestion even at very small sealing flow rates. On the other hand, the results for the steady model with the thin seal approximation show similar trends (for $\Phi_0 > 0.1$) to those for the unsteady simulations. Note that for the single vane pitch model used here, the unsteady large scale structures that occur in the wheel-space [23] at low sealing flow rate are not likely to be predicted correctly.

Also shown in Figure 12 is the theoretical curve obtained from eq (4). The curve was fitted to the computed values obtained from the thin-seal model using the statistical technique of Zhou et al. [4], the values of Φ_{min} and Γ_c being 0.348 and 0.37 respectively.

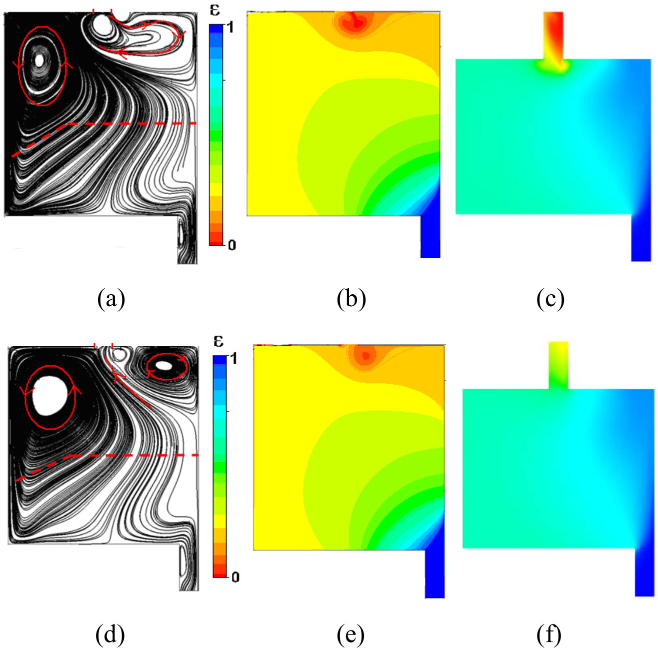

Figure 9. Computed streamlines and time-average effectiveness contours in r-z planes θ = 0 and θ = 0.5 for Φ_0 = 0.022
(a,b) θ = 0, thin seal steady model, (c) unsteady model
(d,e) θ = 0.5, thin seal steady model, (f) unsteady model
The dashed line in figures shows where β = 1

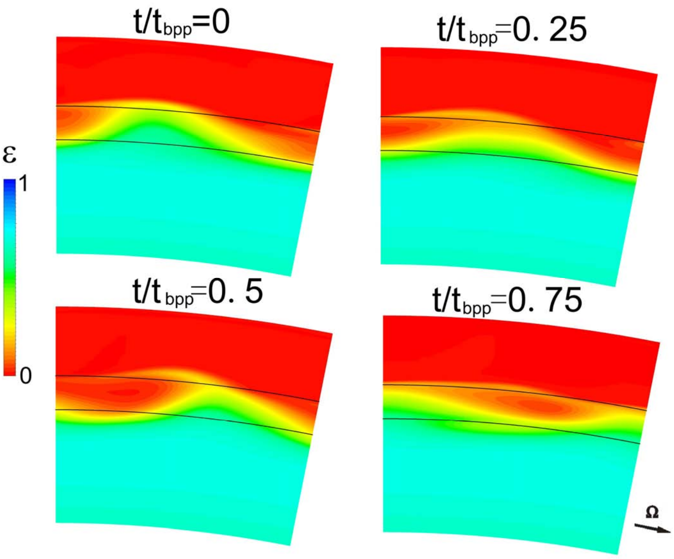

Figure 10. Computed instantaneous contours of effectiveness in the r-θ plane at z/s = 0.5 for the unsteady model for Φ_0 = 0.022

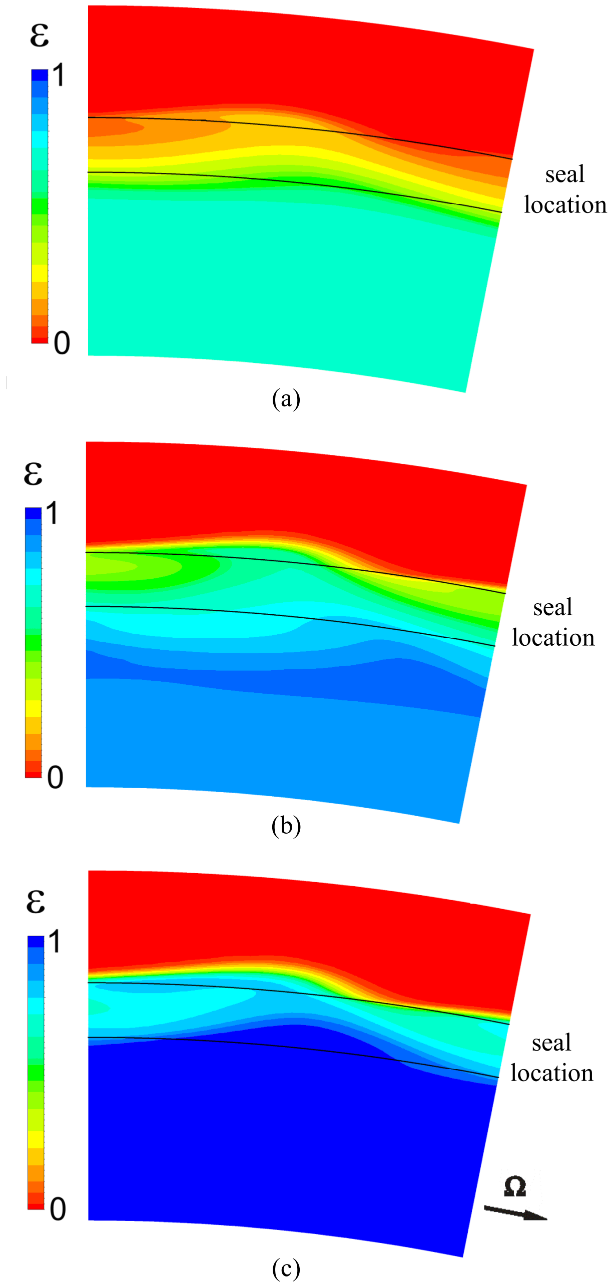

Figure 11. Computed time-average contours of effectiveness in the r-θ plane at z/s = 0.5 for the unsteady model (a) Φ_0 = 0.022, (b) Φ_0 = 0.11, (c) Φ_0 = 0.22

Despite differences in the mixing predicted by the unsteady simulations and the thin seal steady computations, the latter gives comparable effectiveness results to the former (and a broadly similar estimate for Φ_{min}, the minimum value of the sealing flow rate parameter required to prevent ingress) while requiring less than 1/20th of the computing time.

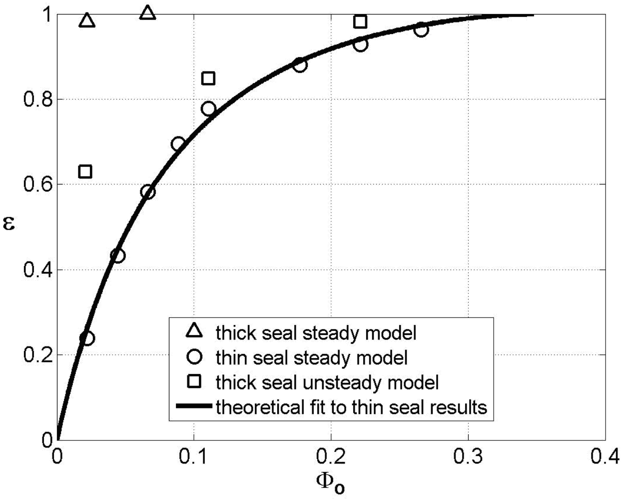

Figure 12. Variation of computed effectiveness with Φ_0 for three different models (the effectiveness is calculated at monitor point 2 in the wheel-space as shown in Figure 2(a))

6. CONCLUSIONS

Unsteady 3D computations have been carried out to investigate the mechanisms of ingestion through an axial clearance turbine rim seal. The influence of unsteady effects in the mainstream annulus have been studied by comparing results with those obtained using simplified steady models. The main findings are summarized below:

- The presence of the blade augments the computed time-average static pressure asymmetry in the annulus caused by the stator vane, though the effects are small.
- As assumed in the orifice model for externally-induced ingress, ingress occurs where the pressure in the annulus is higher than that in the wheel-space and egress occurs where it is lower.
- For the thick seal, unsteady computations predict more ingestion than the corresponding steady computations. This greater exchange of fluid is due mainly to a more well-defined recirculation in the seal clearance region. The region of greatest ingestion follows the circumferential movement of the rotating blade.
- For the thin seal model, the steady computations produce higher levels of ingestion than the thick seal unsteady computations at the larger flow rates.
- The effectiveness equation derived from the orifice model provides a good fit to the effectiveness values computed using the thin-seal model.
- The thin seal results are comparable to those for the unsteady computations while requiring only around 1/20th of the computing time. The thin-seal model might therefore be useful for preliminary design.
- For low sealing flow rates, high swirl ingested fluid is drawn toward the rotor surface. As this would be hot mainstream gas in an engine, this could have serious consequences in practice.
- For the single vane pitch model used here, the unsteady large scale structures that occur in the wheel-space at low sealing flow rate are not likely to be predicted correctly

Future work at the University of Bath will concentrate on further validation by comparing results from the models with experimental results now being obtained. The CFD simulations will then be applied to more practically-relevant seal geometries and operating conditions.

ACKNOWLEDGEMENTS

We wish to thank the China Scholarship Council and Beihang University, Beijing, China, for supporting Kunyuan Zhou during his stay at the University of Bath. He conducted his CFD research using the University of Bath Aquila High Performance Computing facility. The research described here is part of a programme jointly funded by the UK Engineering and Physical Sciences Research Council, Siemens Fossil Power Generation and Siemens Oil & Gas.

REFERENCES

1. Sangan, C.M., Pountney, O.J., Zhou, K., Wilson, M., Owen, J.M. and Lock, G.D., 2011, "Experimental Measurements of Ingress through Turbine Rim Seals. Part 1: Externally-Induced Ingress"; ASME Paper GT2011-45310.
2. Sangan, C.M., Pountney, O.J., Zhou, K., Wilson, M., Owen, J.M. and Lock, G.D., 2011, "Experimental Measurements of Ingress through Turbine Rim Seals. Part 2: Rotationally-Induced Ingress"; ASME Paper GT2011-45313.
3. Owen, J.M., Zhou, K., Pountney, O., Wilson, M. and Lock, G.D., 2010, "Prediction of Ingress through Turbine Rim Seals. Part 1: Externally-Induced Ingress"; ASME Paper GT2010-23346. To appear in ASME J Turbomach.
4. Zhou, K., Wood, S.N. and Owen, J.M., 2011, "Statistical and Theoretical Models of Ingestion through Turbine Rim Seals"; ASME Paper GT2011-45139.
5. Hills, N.J., Chew, J.W. and Turner, A.B., 2002, "Computational and Mathematical Modeling of Turbine Rim Seal Ingestion"; ASME J. Turbomach, vol 124:306-315.
6. Laskowski, G.M., Bunker, R. S., Bailey, J. C., Kapetanovic, S., Itzel, G.M., Sullivan, M.A. and Farrell, T.R., 2009, "An Investigation of Turbine Wheelspace Cooling Flow Interactions with a Transonic Hot Gas Path - Part 2: CFD Simulations"; ASME Paper GT-2009-59193.
7. Rabs, M, Benson, F.-K., Dohmen, H. J. and Schneider, O., 2009, "Investigation of Flow Instabilities near the Rim

Cavity of a 1.5 Stage Gas Turbine"; ASME paper GT2009-59965.
8. Johnson, B.V., Jakoby, R., Bohn, D.E. and Cunat, D., 2009, "A Method for Estimating the Influence of Time-Dependent Vane and Blade Pressure Fields on Turbine Rim Seal Ingestion"; ASME J. Turbomach, Vol. 131, Issue 2, 021005-1 to 10.
9. Wang, C.Z., Johnson, B.V., De Jong, F., Vashist, T.K. and Dutta, R., 2007, "Comparison of flow characteristics in axial-gap seals for close- and wide-spaced turbine stages"; ASME Paper GT2007-27909.
10. Zhou, D., Roy, R., Wang, C. and Glahn, J., 2009, "Main gas ingestion in a turbine stage for three rim cavity configurations"; ASME Paper GT2009-59851.
11. Lewis, P.R. and Wilson, M., 2007, "Three-dimensional computations of ingress in gas turbine cooling systems"; International Gas Turbine Congress, Tokyo, paper TS-040.
12. Mirzamoghadam, A.V., Heitland, G., Morris, M.C., Smoke, J., Malak, M., Howe, J., et al., 2008, "3D CFD Ingestion Evaluation of a High Pressure Turbine Rim Seal Disk Cavity"; ASME Paper GT2008-50531.
13. Mirzamoghadam, A.V., Heitland, G. and Hosseini, K.M., 2009, "The Effect of Annulus Performance Parameters on Rotor-Stator Cavity Sealing Flow"; ASME Paper GT2009-59380.
14. O'Mahoney, T.S.D., Hills, N.J., Chew, J.W. and Scanlon, T., 2010., 2010, "Large-Eddy Simulation of Rim Seal Ingestion"; ASME Paper GT2010-22962.
15. Julien, S., Lefrancois, J., Dumas, G., Boutet-Blais, G., Lapointe, S., Caron, J.-F., et al., 2010, "Simulations of Flow Ingestion and Related Structures in a Turbine Disk Cavity"; ASME Paper GT2010-22729.
16. Dunn, D.M., Zhou, D.W., Squires, K.D., Roy, R.P., Saha, K., Moon, H.K., et al., 2010, "Flow Field in a Single-Stage Model Air Turbine Rotor-Stator Cavity With Pre-Swirled Purge Flow"; ASME Paper GT2010-22869.
17. Green, T. and Turner, A.B., 1994, "Ingestion into the Upstream Wheelspace of an Axial Turbine Stage"; ASME J. Turbomach, Vol. 116, pp 327-332
18. Bohn, D., Rüdzinski, B., Sürken, N. and Gärtner, W., 2000, "Experimental and Numerical Investigation of the Influence of Rotor Blades on Hot Gas Ingestion into the Upstream Cavity of an Axial Turbine Stage"; ASME Paper 2000-GT-284.
19. Menter, F.R., Kuntz, M. and Langtry, R., 2003, "Ten years of industrial experience with the SST turbulence model"; Proc. Turbulence, Heat and Mass Transfer 4.
20. Bohn, D.E., Decker, A., Ohlendorf, N. and Jakoby, R., 2006, "Influence of an Axial and Radial Rim Seal Geometry on Hot Gas Ingestion into the Upstream Cavity of a 1.5-Stage Turbine"; ASME Paper GT2006-90453.
21. Bohn, D., Rudzinski, B., Surken, N., and Gartner, W., 1999, "Influence of Rim Seal Geometry on Hot Gas Ingestion Into the Upstream Cavity of an Axial Turbine Stage"; ASME Paper 99-GT-248.
22. Owen, J.M., Rogers, R. H., 1995, "Flow and Heat Transfer in Rotating-Disc Systems: Volume 2 - Rotating Cavities"; Research Studies Press, John Wiley and Sons.
23. Cao, C., Chew, J.W., Millington, P.R. and Hogg, S.I., 2003, "Interaction of Rim Seal and Annulus Flows in an Axial Flow Turbine"; ASME J. Eng. Gas Turbines and Power, 126, pp. 786–793.

